Research article

Journal of RAMAN SPECTROSCOPY

Received: 17 January 2012 Revised: 16 April 2012 Accepted: 24 April 2012 Published online in Wiley Online Library: 15 July 2012

(wileyonlinelibrary.com) DOI 10.1002/jrs.4116

Raman tensor analysis of hexagonal polyoxymethylene and its application to study the molecular arrangement in highly crystalline electrospun nanofibers

Leonardo Puppulin,[a] Masaya Kotaki,[b] Morimasa Nakamura,[c] Daisuke Iba,[c] Ichiro Moriwaki[c] and Giuseppe Pezzotti[a]*

The orientation dependence in space of Raman-active vibrations in the hexagonal structure of polyoxymethylene (POM) is discussed in terms of Raman tensor elements as intrinsic physical parameters of the lattice. The variation of polarized intensity for the A_1 and the E_1 vibrational modes with respect to the POM molecular orientation is systematically studied, from both theoretical and experimental viewpoints, according to the symmetry assignments of each vibrational mode. A set of working equations including the Raman selection rules associated with the A_1 and the E_1 modes and the orientation distribution function are explicitly formulated and validated by means of a least-square fitting procedure on experimental data. In addition, an approach based on the introduction of orientation distribution functions is applied to quantitatively assess and compare on a statistical base the molecular orientation of two different types of electrospun POM nanofibers. Copyright © 2012 John Wiley & Sons, Ltd.

Keywords: Raman tensor; polyoxymethylene; polarized Raman spectroscopy; molecular orientation; hexagonal structure

Introduction

Nowadays, among thermoplastic polymers for engineering applications, polyoxymethylene (POM, also known as polyacetal) can certainly be considered as one of the most popular and interesting material because of its excellent rigidity, impact toughness, abrasion, creep, and corrosion resistances. For example, POM is often applied to plastic gears, and more than 50% of plastic gears used in mechanical fields are made by POM in Japan. POM is a semicrystalline thermoplastic whose molecular chains pack in two well-known crystallographic systems, the trigonal (t-POM, with hexagonal unit cell) and the orthorhombic (o-POM). Depending upon which conditions prevail at the nucleation stage of crystallization (which may also coincide with the polymerization itself) one may obtain the stable hexagonal form with one molecule per unit cell, or the metastable orthorhombic form with two molecules per unit cell. In the hexagonal crystal, the unit cell contains one helical chain, whose identity period of 17.39 Å (crystallographic *c*-axis) consists of nine chemical units in five turns (9/5 helix). The other unit cell parameter *a* is equal to 4.47 Å.[1] For the t-POM structure, a more detailed (29/16) helical structure was first proposed by Carazzolo.[2] Subsequently, Toshiro *et al*.[3] have refined the crystal structure based on synchrotron X-ray and neutron diffraction data. The orthorhombic form consists of (2/1)-helical molecule. Mortillario *et al*.[4] prepared the first sample of o-POM through polymerization of formaldehyde in aqueous solution. Later, studies conducted by Kobayashi *et al*. and Iguchi showed that o-POM can be obtained as a byproduct of a heterogeneous cationic polymerization of trioxane, which was originally designed for preparing needlelike single crystals of t-POM.[5,6] The properties of POM are significantly influenced by the crystal morphology of the polymer. From a morphological point of view, the crystal structure of the crystalline phase might be classified into two types: a folded-chain or lamellar crystal and an extended-chain crystal (ECC), depending on the crystallization conditions and sample processing.[7] A typical folded-chain or lamellar crystal sample can be prepared by crystallization from dilute solution (i.e. bromobenzene) obtaining hexagon-shaped lamellar crystals with a thickness of about 10 nm.[8] On the other hand, drawing a POM fiber is one way to develop the ECC-type structure. The crystal morphology in melt-grown bulk samples might experience structures between the above two extremes. Electrospinning is a cost effective method to produce novel polymer fibers whose diameters range from a few nanometers to several microns; the smaller the fiber diameter, the better its mechanical properties (e.g. tensile modulus and strength). High specific surface area of ultrafine fibers is desirable for the development of filtration membranes and for protective clothing

* *Correspondence to: Giuseppe Pezzotti, Ceramic Physics Laboratory, Kyoto Institute of Technology, Matsugasaki, Sakyo-ku, Kyoto 606-8585, Japan. E-mail: pezzotti@kit.ac.jp*

a *Ceramic Physics Laboratory, Kyoto Institute of Technology, Matsugasaki, Sakyo-ku, Kyoto, 606-8585, Japan*

b *Department of Advanced Fibro-Science, Kyoto Institute of Technology, Matsugasaki, Sakyo-ku, Kyoto, 606-8585, Japan*

c *Department of Mechanical and System Engineering, Kyoto Institute of Technology, Matsugasaki, Sakyo-ku, Kyoto, 606-8585, Japan*

that would restrict airborne chemicals. Additionally, electrospun fibers can be used in biomedical applications such as prosthesis and drug delivery devices. Recently, Kongkhlang *et al.*[9] have produced electrospun POM nanofibers and demonstrated that, by controlling the spinning electrical voltage and rotating speed of the disk rotator, it is possible to control both crystal morphology and molecular orientation. In both the far and recent past, the morphology of ECC-POM and other highly oriented polymer fibers have been studied using various techniques such as microscopy, electron diffraction and infrared (IR) spectroscopy.[3,10–12] Small-angle X-ray scattering has also been used to obtain some morphological information, but it is quite difficult to measure the small-angle X-ray scattering pattern for a thin fiber using X-ray diffraction on a laboratory level. The IR spectroscopic technique is considered as a good analytical method for POM, because the infrared spectrum of POM is quite sensitive to structural features, as already shown by several authors.[7,11–13] Similar to IR spectroscopy, Raman spectroscopy is also a powerful tool for the analysis of molecular structure and, furthermore, the availability of selection rules for Raman scattering involves several advantages over IR. Both spectroscopic techniques can be used to calculate the orientation distribution function (ODF), which shows the statistical distribution of molecules oriented with respect to a certain direction of the material, but while Raman spectroscopy enables one to determine both second and fourth terms in the expansion of ODF, IR contains only information regarding the second term.[14] Moreover, it is possible to collect Raman spectra from a micron-sized region of a sample when the technique is combined with optical microscopy. The electric vector of the Raman scattered light and the incident light are both correlated through a characteristic Raman tensor, which is unique for each Raman-active molecular vibrational mode. The concept of the Raman tensor for Raman spectroscopy was first established according to Ovander[15] in 1960. The concept was based on molecular symmetry and was further correlated with crystal structures by Loudon in 1964.[16] The theoretical approach given by Loudon, as also used in this paper, expresses the intensity of the Raman bands according to a set of selection rules (i.e. functions giving the angular variations of the observed Raman scattering for a given lattice vibration and symmetry), which in turn obey a second-rank tensor.[15,16] Group theory then enables to predict which Raman transitions can be observed and to determine which components of the Raman tensors will not vanish.

In this paper, we first present a complete theoretical description of the periodic dependences under polarized light of the A_1 and E_1 phonon-mode intensities on the set of three Euler angles comprised between the laser polarization direction and the crystallographic axes of the hexagonal structure of POM. Then, we validate the obtained Raman selection rules with experimental data collected by performing a set of polarized Raman experiments on highly oriented electrospun POM nanofibers. By fitting the experimental polarized Raman intensity collected at different azimuthal angles, we also calculate a set of three independent Raman tensor components. In doing so, we shall introduce the ODF in its general expression to link the polarized Raman intensity, as given in the Loudon's formalism,[16] to the statistical distribution of the molecular chain directions along the long axis of the fiber. The obtained results are finally used to characterize the orientational order of two types of electrospun POM nanofibers produced by applying different velocities to the rotating disk collector during preparation.

Experimental technique

Two types of electrospun POM nanofibers have been analyzed by means of micro-Raman spectroscopy. 12 wt% POM solutions with hexafluoroisopropanol were prepared, which resulted in clear and homogeneous solutions. The solutions were electrospun into nanofibers at an electrical voltage of 15 kV. The electrospun POM fibers were deposited onto a rotating disk collector, where the tip-to-collector distance was fixed at 10 cm and the volumetric flow rate was 0.5 mL/h. Spinning was performed under a relative humidity of 50% and at a temperature of 26 °C. The velocity of the rotating disk collector was varied for the two types of nanofiber under investigation: 1000 min^{-1} (i.e. 630 m/min in take-up velocity) and 3000 min^{-1} (1890 m/min) (henceforth referred to as samples A and B, respectively). Each electrospun POM membrane was dried in a desiccator prior to spectroscopic analysis.

The spectra were collected at room temperature by a triple-monochromator (T-64000, Jobin-Yvon/Horiba Group, Kyoto, Japan) equipped with a charge-coupled device detector, and analyzed by using commercially available software (LABSPEC, Horiba/Jobin-Yvon, Kyoto, Japan). A spectral resolution of 0.15 cm^{-1} was achieved by means of an 1800 grating L/mm. The laser excitation source was a monochromatic blue line emitted by an Ar-ion laser at a wavelength of 488 nm (Stabilite 2017-Spectra Physics, Mountain View, CA) with a power of 100 mW. Spectra were collected in backscattering geometry using sheet polarizers in both cross and parallel configurations with respect to the incident laser polarization vector. Spectral integration times were typically 5 and 15 s for parallel-polarized and cross-polarized spectra, respectively, and the recorded signal was averaged over three successive measurements. In Figs 1(a) and (b), a schematic draft is shown that explains the experimental set-up adopted for our spectroscopic study of the POM fibers and our choice of laboratory reference system with respect to the crystal reference system in terms of Euler angles in space, respectively.

Experimental results and discussion

A literature survey of the studies published in the past decades,[7,11–13,17,18] which were mainly based on wide-angle X-ray measurements, IR spectroscopy and scanning electron microscopy analysis, brings about evidence that POM fibers generally possess higher degree of uniaxial molecular orientation and higher crystallinity as compared with bulk POM samples. The crystalline phase in the fiber is predominantly hexagonal and, because of the strongly unidirectional deformation that takes place during processing, POM molecular chains (i.e. the *c*-axis of the hexagonal cell) are highly aligned along the axis of the fiber. In this study, we matched highly spectrally resolved (polarized) Raman data with a structural model proposed by Kongkhlang *et al.* for describing the morphology of electrospun POM nanofibers on the mesoscale.[12] According to those researchers, stretching during the electrospinning process triggers the formation of the ECC morphology in the nanofibers. Moreover, a single nanofiber is described as a bundle of nanofibrils arranged along the fiber axis, whose diameter decreases with increasing the velocity of the rotating disk collector. From a spectroscopic viewpoint, the vibrational Raman spectrum of POM has been the subject of a large number of research studies during the past 50 years. Kobayashi *et al.* measured the polarized Raman spectra of t-POM by means of a microprobe technique.[7]

Journal of RAMAN SPECTROSCOPY

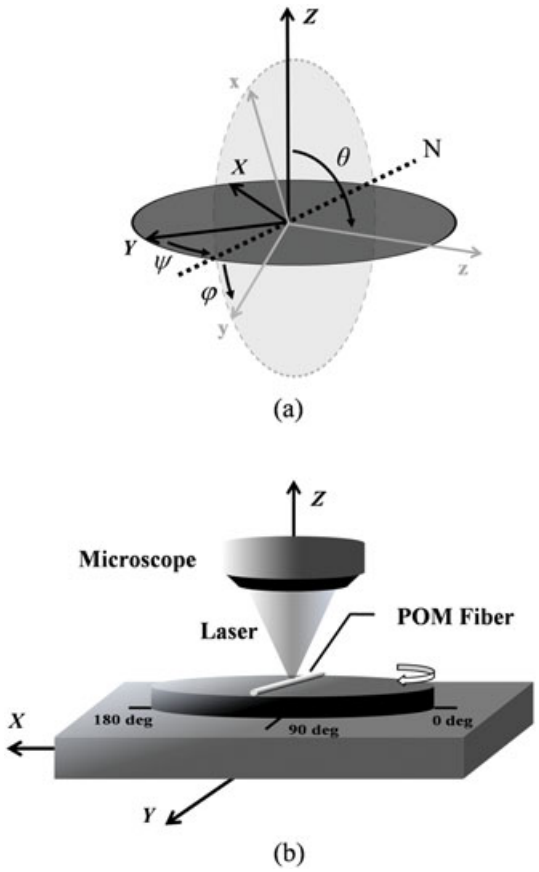

Figure 1. A schematic draft of the adopted Cartesian reference system is shown in (a), with the Euler angles that correlate the laboratory reference system (*XYZ*) to the crystallographic reference system (*xyz*) of the POM crystalline structure. (b) Schematic of the rotating jig utilized to collect Raman band intensities at different angles between the fiber axis and the laser polarization direction.

Regarding the crystallographic structure, the most reliable hypothesis for space group of t-POM is $P3_1$–C_3^2 or $P3_2$–C_3^3. The zone-center normal modes of the 9/5 helical molecule of t-POM are classified into six irreducible representations: A_1, A_2, E_1, E_2, E_3, and E_4 species, where the A_2 and E_1 modes are IR-active, the A_1, E_1, and E_2 modes are Raman active while the E_3 and E_4 are inactive in both spectroscopies.[13,19–21] Figure 2 shows a typical Raman spectrum of POM collected from electrospun nanofibers in the range between 500 and 1200 cm^{-1} (in terms of Raman shift). The peak positions labeled in Fig. 2 correspond to the assignments of hexagonal POM as reported in literature.[13,19–21] The hexagonal unit cell of t-POM belongs to a polar space group ($P3_1$–C_3^2 or $P3_2$–C_3^3); therefore, the E_l Raman modes might give rise to band splitting into the LO (longitudinal optic) and TO (transverse optic) modes.[20] As shown in Fig. 2, in the spectra collected from the nanofiber under investigation, both the components of the doubly degenerate species clearly appear around 937 and 1095 cm^{-1} (see the doublets located at 949 (LO) and 937 (TO) cm^{-1}, and 1106 (LO) and 1096 (TO) cm^{-1}, respectively). Moreover, the 542 cm^{-1} band assigned to the only hexagonal structure is clearly visible, while no bands characteristic of the orthorhombic structure were detected in our experiment. Therefore, according to these spectral features, we conclude that the investigated fibers belong to the hexagonal t-POM structure.

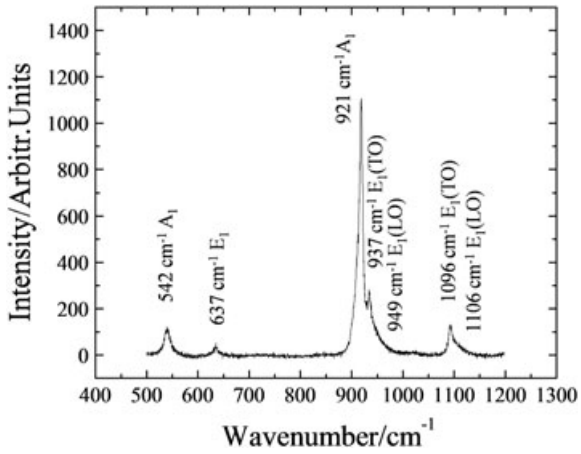

Figure 2. Typical Raman spectrum of hexagonal POM collected from electrospun nanofibers in the range between 500 and 1200 cm^{-1} (in terms of Raman shift). The present investigation focused on two bands belonging to the A_1 mode located at 921 cm^{-1} and to the E_1 mode located at 1096 cm^{-1}.

The tensorial rules governing the relative intensity of Raman bands for a given crystal structure can be expressed as a function of crystal orientation in space and probe polarization geometry,[22,23] according to the following tensorial equation:

$$I \propto |e_i \Re e_s|^2 \tag{1}$$

where I is the scattered Raman intensity, e_i and e_s are the unit polarization vectors of the electric field for incident and scattered light, respectively. For a fixed polarization vector of the incident light (which is the case of our Raman equipment), parallel and cross polarization geometries are thus possible for collecting the scattered light, the unit polarization vectors being expressed in Cartesian coordinates, as follows:

$$e_{i\ xyz}^{\parallel} = (0 \quad 1 \quad 0), \qquad e_{s\ xyz}^{\parallel} = \begin{pmatrix} 0 \\ 1 \\ 0 \end{pmatrix}, \qquad e_{s\ xyz}^{\perp} = \begin{pmatrix} 1 \\ 0 \\ 0 \end{pmatrix} \tag{2}$$

where the subscripts 'i' and 's' refer to incident and scattered light, respectively; the superscripts $\parallel$ and $\perp$ refer to the parallel and the cross configuration of the polarized probe, respectively $Z(YY)\bar{Z}$ and $Z(YX)\bar{Z}$, respectively, according to Porto notations[24]). $\Re$ is a second-rank Raman scattering tensor, different for each vibrational mode. In the present analysis, we considered the POM Raman bands located at 637, 921, and 1096 cm^{-1}. These bands are related to O–C–O bending (E_1 mode), C–O–C symmetric stretching (A_1 mode), and C–O–C asymmetric stretching (E_1(TO) mode) vibrations, respectively. The pertinent Raman tensors expressed in the hexagonal crystal principal axes, are as follows:

$$\Re_{A_1} = \begin{bmatrix} a & 0 & 0 \\ 0 & a & 0 \\ 0 & 0 & b \end{bmatrix}, \Re_{E_1(x)} = \begin{bmatrix} 0 & 0 & 0 \\ 0 & 0 & c \\ 0 & c & 0 \end{bmatrix}, \Re_{E_1(y)} = \begin{bmatrix} 0 & 0 & -c \\ 0 & 0 & 0 \\ -c & 0 & 0 \end{bmatrix} \tag{3}$$

where a, b, and c are usually referred to as the Raman tensor elements. The intensity of the E_1 mode consists of two components, $E_1(x)$ and $E_1(y)$. However, the related bands are fully

overlapping, which leads to a cumulative Raman intensity of the two-mode component described by the following equation[16]:

$$I_{E_1}^{\parallel,\perp} = xI_{E_1(x)}^{\parallel,\perp} + (1-x)I_{E_1(y)}^{\parallel,\perp} \quad (4)$$

The above Eqn (4) is valid for both parallel and cross configurations (cf. superscripts) and the weight parameter, x, can be assumed equal to 0.5, according to band symmetry arguments.[25] Upon substituting for Eqn (3) in Eqn (1), we find

$$I_{A_1}^{\parallel} = \Lambda\left[\begin{array}{l} b\sin^2\theta\sin^2\psi + a(\cos\psi\sin\varphi + \cos\theta\cos\varphi\sin\psi)^2 + \\ +a(\cos\varphi\cos\psi - \cos\theta\sin\varphi\sin\psi)^2 \end{array}\right]^2 + \gamma \quad (5)$$

$$I_{A_1}^{\perp} = \Lambda\left[-(a-b)\cos\psi\cos^2\theta\sin\psi\right]^2 + \gamma \quad (6)$$

$$I_{E_1(x)}^{\parallel} = \Lambda[2c\sin\theta\sin\psi(\cos\varphi\cos\psi - \cos\theta\sin\varphi\sin\psi)]^2 + \gamma \quad (7)$$

$$I_{E_1(y)}^{\parallel} = \Lambda[-2c\sin\theta\sin\psi(\sin\varphi\cos\psi + \cos\theta\cos\varphi\sin\psi)]^2 + \gamma \quad (8)$$

$$I_{E_1(x)}^{\perp} = \Lambda[c\sin\theta(\cos\varphi\cos2\psi - 2\cos\theta\cos\psi\sin\varphi\sin\psi)]^2 + \gamma \quad (9)$$

$$I_{E_1(y)}^{\perp} = \Lambda\left[c\sin\theta\left(-\sin\varphi\cos^2\psi - 2\cos\theta\cos\varphi\cos\psi\sin\psi + \sin\varphi\sin^2\psi\right)\right]^2 + \gamma \quad (10)$$

For the two E_1 modes considered in this study, the values of the c parameter might differ and in the remainder of this paper we will indicate with c the values calculated for the 637 cm^{-1} band, while c' is the Raman tensor parameter retrieved from the 1096 cm^{-1} band. In Eqns (5)–(10), Λ and γ represent numerical constants that depend on the instrumental configuration and polarization geometry. Moreover, the selection rules invariably show that the periodicity of the Raman intensity fluctuation could be expected either over an interval $0 \le \psi \le \pi$ or $0 \le \psi \le \pi/2$, depending on the examined Raman mode. Figure 3 shows the Raman band located at 921 cm^{-1} (A_1), as collected from sample B for different polarization geometries and at different azimuthal angles, ψ. In our reference choice (cf. Fig. 1), θ is expected to be very close to $\pi/2$ (i.e. given the expected high degree of alignment of the fiber), ψ corresponds to the in-plane rotation angle of the jig supporting the fiber, namely it is the variable angle in our experiments, while φ is the angle describing the orientation of the a-axis in the c-plane, which is unknown and might be different for each fibril of which the nanofiber is made up. Nevertheless, the high alignment of POM molecular chains renders the fiber a suitable sample to fully resolve the second-rank tensor associated with the vibrational bands of the hexagonal structure. In fact, the c-axis of the hexagonal structure is highly oriented along the fiber axis, while Eqns (4)–(9) are invariant with respect to a-axis orientation, which lies on the fiber cross-section plane. In other words, when θ is equal to $\pi/2$, the azimuthal angular dependence of the scattered polarized intensity collected from the nanofiber is independent of φ angle. However, to obtain a fully quantitative Raman assessment, the local orientation distribution function of the molecular chains has to be taken into consideration in the computational procedure.[26–28] Such a function has been formulated in terms of

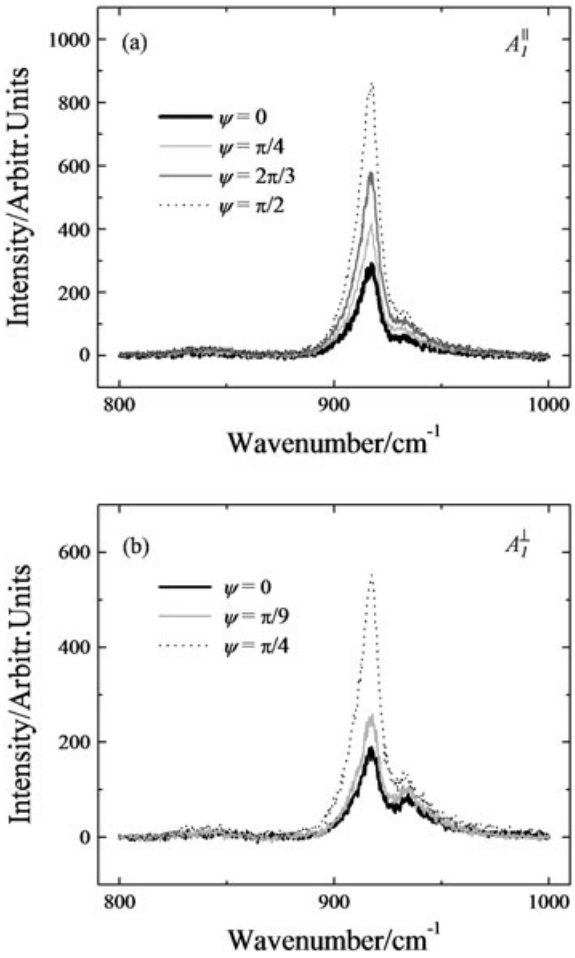

Figure 3. A_1 Raman band located at 921 cm^{-1}, as collected from sample B in parallel (a) and cross (b) probe polarization geometries, as a function of rotation angle ψ.

Wigner functions expanded in a series of Legendre polynomials. A set of our working equations that include both Raman selection rules and molecular distribution patterns can be given as follows[29]:

$$I_{A_1}^{\parallel,\perp}(\theta,\phi,\psi) = \frac{\int_{\gamma=0}^{\gamma=2\pi}\int_{\alpha=0}^{\alpha=2\pi}\int_{\beta=0}^{\beta=\pi} I_{A_1}^{\parallel,\perp}(\theta,\phi,\psi)f(\beta)\sin\beta d\beta d\alpha d\gamma}{\int_{\gamma=0}^{\gamma=2\pi}\int_{\alpha=0}^{\alpha=2\pi}\int_{\beta=0}^{\beta=\pi} f(\beta)\sin\beta d\beta d\alpha d\gamma} \quad (11)$$

$$I_{E_1}^{\parallel,\perp}(\theta,\phi,\psi) = \frac{\int_{\gamma=0}^{\gamma=2\pi}\int_{\alpha=0}^{\alpha=2\pi}\int_{\beta=0}^{\beta=\pi} I_{E_1}^{\parallel,\perp}(\theta,\phi,\psi)f(\beta)\sin\beta d\beta d\alpha d\gamma}{\int_{\gamma=0}^{\gamma=2\pi}\int_{\alpha=0}^{\alpha=2\pi}\int_{\beta=0}^{\beta=\pi} f(\beta)\sin\beta d\beta d\alpha d\gamma} \quad (12)$$

with the Raman intensities in the triple integrals given in Eqns (5)–(10). As described in detail in a previous paper,[30] (α,β,γ) represent an additional set of Euler angles that describes the molecular orientation with respect to the axes of preferential orientation within the probe. The set of Euler angles (θ,φ,ψ) describing the orientation of the generic molecule in space can be expressed in terms of $(\alpha,\beta,\gamma)$and(θ_p,ϕ_p,ψ_p), which is the set of angles describing the preferential orientation within the probe. Because of the high alignment of the molecular chains in the nanofibers, θ_p can be considered equal to $\pi/2$ and ψ_p equal to the azimuthal rotation angle of the fiber

axis. Moreover, φ_p can be neglected in the calculation when θ is close to $\pi/2$. The orientation distribution function, $f(\beta)$, is given as

$$f(\beta) = A\exp\{-[\lambda_2 P_2(\cos\beta) + \lambda_4 P_4(\cos\beta)]\} \quad (13)$$

where A is a constant and the parameters λ_2 and λ_4 are the Lagrange multipliers used in the definition of the principle of maximum information entropy reported by Jaynes.[31] The three parameters A, λ_2 and λ_4 can be determined by solving the system of three equations, which describe the average values of the Legendre polynomials

$$\int_{\gamma=0}^{\gamma=2\pi}\int_{\alpha=0}^{\alpha=2\pi}\int_{\beta=0}^{\beta=\pi} f(\alpha,\beta,\gamma)\sin\beta d\beta d\alpha d\gamma = 1 \quad (14)$$

$$\int_{\gamma=0}^{\gamma=2\pi}\int_{\alpha=0}^{\alpha=2\pi}\int_{\beta=0}^{\beta=\pi} P_2(\cos\beta)f(\beta)\sin\beta d\beta d\alpha d\gamma = \langle P_2(\cos\beta)\rangle \quad (15)$$

$$\int_{\gamma=0}^{\gamma=2\pi}\int_{\alpha=0}^{\alpha=2\pi}\int_{\beta=0}^{\beta=\pi} P_4(\cos\beta)f(\beta)\sin\beta d\beta d\alpha d\gamma = \langle P_4(\cos\beta)\rangle \quad (16)$$

Of the two 'order parameters', $\langle P_2(\cos\beta)\rangle$ and $\langle P_4(\cos\beta)\rangle$, the former is usually referred to as the Hermans orientation parameter.[29] This parameter assumes the value 0 when the orientation of the orthorhombic crystals is fully random, while values 1 and −0.5 are experienced when a perfect orientation is reached along and perpendicular to a given axis (e.g. the long axis of the fiber), respectively. The Hermans orientation parameter is the primary parameter to judge about the alignment of crystalline patterns.[29]

In the computational practice, depending on the band under consideration, the number of unknown parameters varies from a total of four to a total of five, namely the Raman tensor elements (i.e. c or c' for the two E_1 modes, a and b for the A_1 mode), two Lagrange multipliers, λ_2, and λ_4, and one instrumental constant (Λ vanishes using normalized Raman intensities, while γ remains as a fitting parameter) need to be determined. On the other hand, the two order parameters, $\langle P_2(\cos\beta)\rangle$ and $\langle P_4(\cos\beta)\rangle$, and the constant A can be obtained from the additional Eqns (14)–(16). Accordingly, for fully retrieving all the unknown parameters, a series of $n > 5$ Raman spectra taken at different ψ angles of each location in the in-plane angular interval $0 < \psi < \pi/2$ is needed. A computer routine was then run to obtain least-squares fitting curves to experimental plots that, in the present experimental protocol, included $n = 9$ angular values (i.e. thus exceeding the minimum number $n = 5$ of needed spectral rotations). It should be noted that the computational routine should locate four tensor elements whose values are independent of the probed location and the type of fiber, being parameters intrinsic to the crystal

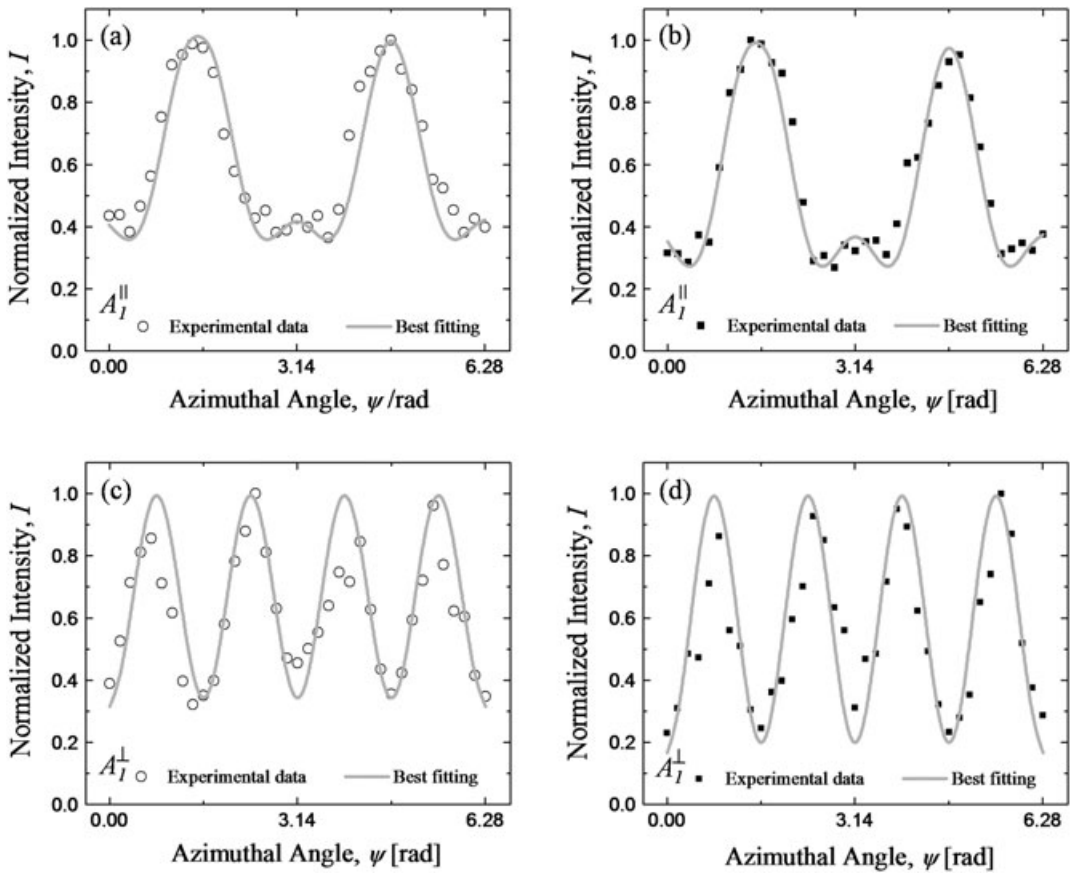

Figure 4. Angular dependences of the Raman intensity at 921 cm^{-1} retrieved in parallel polarization from samples A and B (in (a) and (b), respectively). Least-squares fitting curves were obtained according to Eqns (5) and (6). Similarly, in (c) and (d) the angular dependences collected in cross polarization on sample A and B, respectively, are reported.

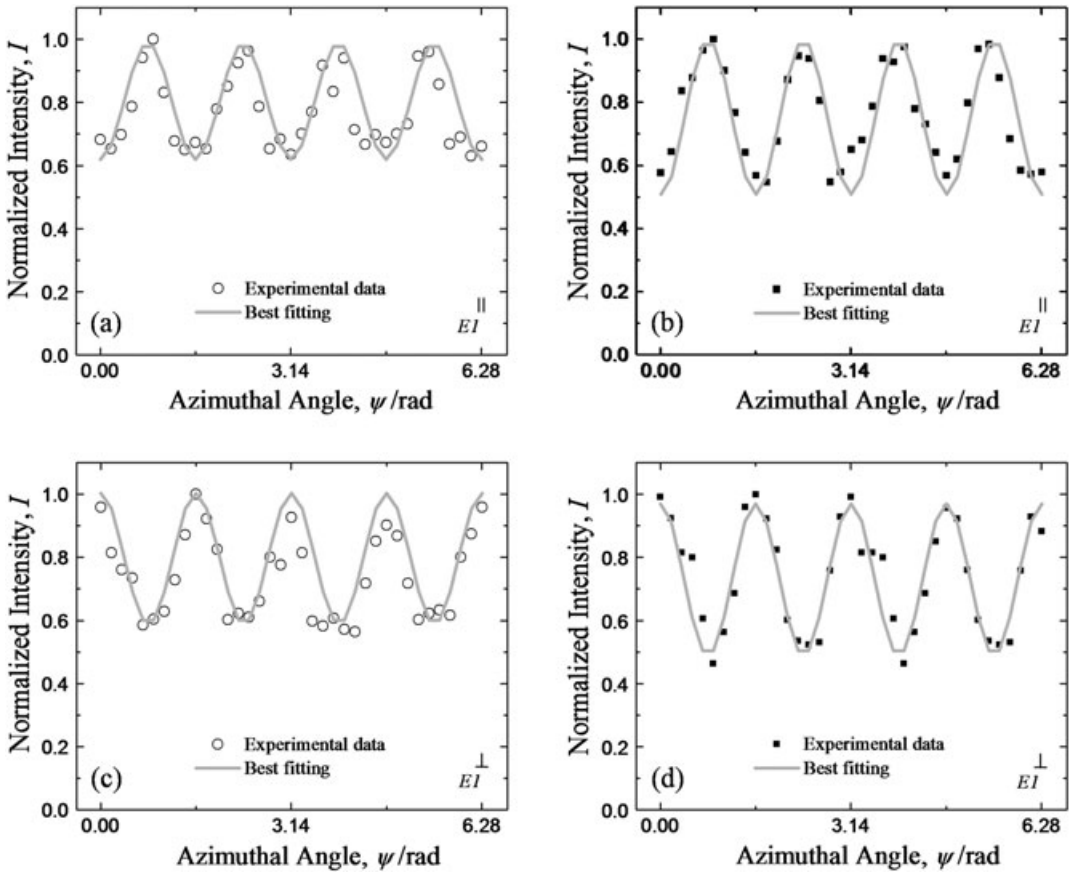

Figure 5. Angular dependences of the Raman intensity at 1096 cm^{-1} as retrieved in parallel polarization on samples A and B (in (a) and (b), respectively). Least-squares fitting curves were obtained according to Eqns (7) and (8). Similarly, in (c) and (d) the angular dependences collected in cross polarization from sample A and B, respectively, are reported.

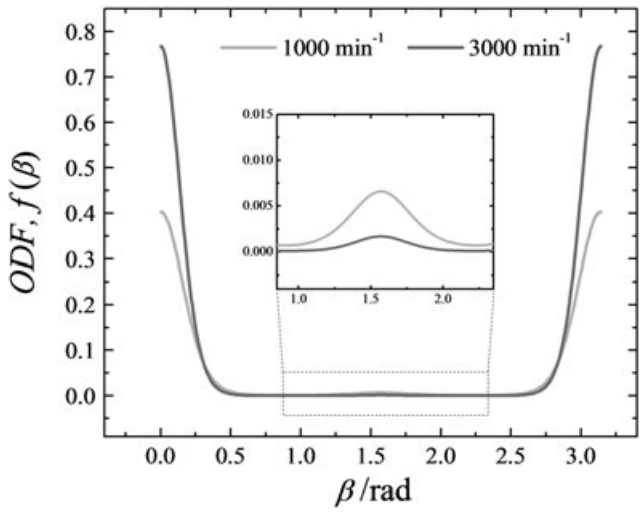

Figure 6. Orientation distribution functions as calculated from experimental data collected from the two types of electrospun nanofibers (referred to as sample A and B throughout the text), which differed for the velocity of the rotating disk collector.

structure. On the other hand, the other unknown parameters should be location dependent. Typical angular dependencies and their related best fitting curves experimentally retrieved from sample A and B are shown in Figs 4 and 5 for A_1 and E_1 (1096 cm^{-1}) modes, respectively. The least-squares fitting of the experimental periodic dependencies (according to Eqns (5)–(10)) led to values −0.362, –0.934, 0.692, and 0.622 for the Raman tensor elements *a*, *b*, *c* and *c*′ respectively. These values represent an average of data collected at 10 random locations on an isolated fiber. Average orientation distribution functions, as obtained for the two types of electrospun nanofibers, are plotted in Fig. 6. The values of the Hermans parameters are listed in Table 1 and represent the average calculated from the three bands on a set of data collected at 10 random locations on each sample. These results confirm the extremely high degree of alignment of the POM structure along the long axis of the fiber and the possibility of controlling the morphology, namely the degree of unidirectional molecular alignment, by means of the processing condition of the electrospinning technique.

Table 1. Numerical parameters characterizing the orientation distribution functions plotted in Fig. 6

	$\langle P_2(\cos\beta)\rangle$	$\langle P_4(\cos\beta)\rangle$	*A*	λ_2	λ_4
1000 rpm	0.73	0.65	0.0028	−1.24	−3.72
3000 rpm	0.90	0.79	0.0005	−5.06	−2.04

Conclusions

In conclusion, a sensitivity study of the Raman selection rules for the hexagonal structure of highly aligned POM fibers, considering three Euler angles in space and the role of orientation distribution functions, has allowed us to unfold a set of three Raman tensor elements and confirm the validity of a structural model proposed by previous authors, involving the existence of a fibrillar structure in electrospun nanofiber whose degree of alignment along the fiber axis can be controlled by the processing conditions. The knowledge of the set of Raman tensor elements opens the possibility of quantitatively evaluating unknown orientation patterns for POM molecular chains in space by means of polarized Raman spectroscopy.

References

[1] H. Todokoro, S. Yasumoto, S. Murahashi, I. Nitta, *J. Polym. Sci.* **1960**, *44*, 266.
[2] G. Carazzolo, *J. Polym. Sci. A* **1960**, *1*, 1573.
[3] K. Toshiro, T. Kamae, H. Asanaga, T. Oikawa, *Macromolecules* **2004**, *37*, 826.
[4] L. Mortillario, G. Galliazzo, S. Bessi, *Chem. Ind.* **1964**, *46*, 139.
[5] M. Kobayashi, Y. Itoh, H. Todokoro, M. Shimomura, M. Iguchi, *Polym. Commun.* **1987**, *29*, 351.
[6] M. Iguchi, *Polymer* **1983**, *24*, 915.
[7] M. Kobayashi, M. Sakashita, M. Hasegawa, *Macromolecules* **1991**, *24*, 4796.
[8] D. C. Bassett, F. R. Dammont, R. Salovey, *Polymer* **1964**, *5*, 579.
[9] T. Kongkhlang, M. Kotaki, Y. Kousaka,T. Umemura, D. Nakaya, S. Chirachanchai, *Macromolecules* **2008**, *41*, 4746.
[10] D. Snetivy, G. J. Vancso, *Macromolecules* **1992**, *25*, 3320.
[11] M. Kobayashi, M. Sakashita, *J. Chem. Phys.* **1992**, *96*(1), 748.
[12] T. Kongkhlang, K. Tashiro, M. Kotaki, S. Chirachanchai, *J. Am. Chem. Soc.* **2008**, *130*, 15460.
[13] M. Shimomura, M. Iguchi, M. Kobayashi, *Polymer* **1990**, *31*, 1406.
[14] M. vanGurp, *Colloid Polym. Sci.* **1995**, *273*, 607.
[15] L. N. Ovander, *Opt. Spectrosc.* **1960**, *9*, 302.
[16] R. Loudon, *Adv. Phys.* **1964**, *13*, 423.
[17] T. Komatsu, *J. Mater. Sci.* **1993**, *28*, 3043.
[18] T. Komatsu, S. Enoki, A. Aoshima, *Polymer* **1991**, *32*(11), 11.
[19] M. Kobayashi, H. Morishita, M. Shimomura, M. Iguchi, *Macromolecules* **1987**, *20*, 2453.
[20] M. Shimomura, M. Iguchi, M. Kobayashi, *Polymer* **1988**, *29*, 351.
[21] H. Morishita, M. Kobayashi, F. Kaneko, *Macromolecules* **1994**, *27*, 5907.
[22] G. Turrell, in Practical Raman Spectroscopy, (Eds: D. J. Gardiner, P. R. Graves), Springer, Berlin, **1989**, p. 13.
[23] M. S. Amer, J. Maguire, L. Cai, R. Biggers, J. Busbee, S. R. LeClair, *J. Appl. Phys.* **2001**, *89*, 8030.
[24] K. Nakamoto, Infrared and Raman spectra of inorganic and coordination compounds, Wiley-Interscience, New York, **1986**.
[25] S. P. S. Porto, R. S. Krishnan, *J. Chem. Phys.* **1967**, *47*, 1009.
[26] M. Pigeon, R. E. Prud'homme, M. Pézolet, *Macromolecules* **1991**, *24*, 5687.
[27] M. J. Citra, D. B. Chase, R. M. Ikeda, K. H. Gardner, *Macromolecules* **1995**, *28*, 4007.
[28] G. Y. Nikolaeva, L. E. Semenova, K. A. Prokhorov, S. A. Gordeyev, *Laser Phys.* **1997**, *7*(2), 403.
[29] R. Pérez, S. Banda, Z. Ounaies, *J. Appl. Phys.* **2008**, *103*, 074302.
[30] L. Puppulin, Y. Takahashi, W. Zhu, N. Sugano, G. Pezzotti, *Acta Biomater.* **2011**, (3), 1150–1159.
[31] E. T. Jaynes, *Phys. Rev.* **1957**, *106*, 620.